MATERIALS CHEMISTRY
FRONTIERS

RESEARCH ARTICLE

View Article Online
View Journal | View Issue



Cite this: *Mater. Chem. Front.*, 2025, **9**, 676

# Achieving dual-mode long-persistence afterglow through an aromatic furan organic host–guest system†

Zheng Gong, Qingyang Cui, Xiancheng Nie, Guoqing Zhang * and Biao Chen *

Received 8th November 2024,
Accepted 6th January 2025

DOI: 10.1039/d4qm00977k

rsc.li/frontiers-materials

Pure organic long-persistence luminescence has recently garnered significant attention due to its diverse potential applications. Nonetheless, the attainment of pure organic dual-mode long-persistence afterglow with high efficiency remains a significant challenge. Herein, we report the successful realization of high-efficiency, color-tunable dual-mode room-temperature phosphorescence (RTP) along with thermally activated delayed fluorescence (TADF) of approximately 50 ms, utilizing an aromatic furan organic host–guest system. Our investigation into this system reveals two key findings: (1) the heavy-atom effect of the host and guest molecules plays distinct roles in modulating the efficiency of the intersystem crossing (ISC) and reverse intersystem crossing (RISC) processes; and (2) the dual-mode long-persistence luminescence can be effectively adjusted by manipulating the energy gap between the excited triplet states of host and guest molecules. Additionally, we demonstrated the capability for color display utilizing this host–guest system through inkjet printing.



## Introduction

Long-persistence luminescent materials represent a category of substances capable of absorbing energy and continuing to emit light even after the excitation source is removed. These materials hold significant promise for applications in nighttime emergency signaling, anti-counterfeiting measures, information storage, and clinical diagnostics.[1–7] To date, the majority of commercially available long-persistence luminescent materials are primarily derived from inorganic salts, such as silicate and aluminate systems, or from transition metal complexes, including those involving iridium and platinum. However, these inorganic systems exhibit limitations in terms of flexibility, processability, and color purity, while transition metal systems raise concerns regarding cost and environmental impact.[8–12] In contrast, organic phosphors are structurally flexible, spectroscopically tunable, stimuli-responsive, and environmentally friendly, making them excellent candidates for further exploration. Recently, there has been considerable progress in the development of pure organic long-persistence luminescent materials,[13–18] which have begun to address these limitations and serve as viable alternatives to traditional inorganic and transition metal-based systems.

*Hefei National Laboratory for Physical Sciences at the Microscale, University of Science and Technology of China, Hefei, 230026, P. R. China.*
*E-mail: gzhang@ustc.edu.cn, biaochen@ustc.edu.cn*

† Electronic supplementary information (ESI) available. See DOI: https://doi.org/10.1039/d4qm00977k

Pure organic long-persistence luminescent materials can be categorized into thermally activated delayed fluorescence (TADF)[19–21] and room-temperature phosphorescence (RTP), both of which involve the modulation of the photophysical processes associated with excited triplet states.[22–27] Over the past few decades, various design strategies have been proposed to achieve high-efficiency long-persistence luminescence, focusing on increasing the stable excited triplet population and suppressing nonradiative transitions. These strategies include host/guest complexation, crystallization, halogen bonding, charge transfer states, H-aggregation, and chromophore confinement.[28–36] Significant research milestones have emerged, particularly from guest–host doped systems, contributing to advancements in diverse fields such as next-generation optoelectronics, high-contrast bioimaging, chiral recognition, anti-counterfeiting, and optical sensors.[37–46] However, reports on dual-mode long-persistence luminescence remain scarce, and most existing materials focus on single-component systems with complex structures that require special crystallization, thereby limiting their practical applications.[47,48]

Herein, we present the construction of a series of host–guest systems utilizing aromatic furan molecules with high luminescence yield and photostability (structures depicted in Fig. 1), which enables the achievement of highly efficient and color-tunable dual-mode RTP alongside TADF with a duration of approximately 50 ms. Additionally, we conduct further experiments to address the following scientific questions: (1) how to balance the heavy atom effect within the host–guest system,

 

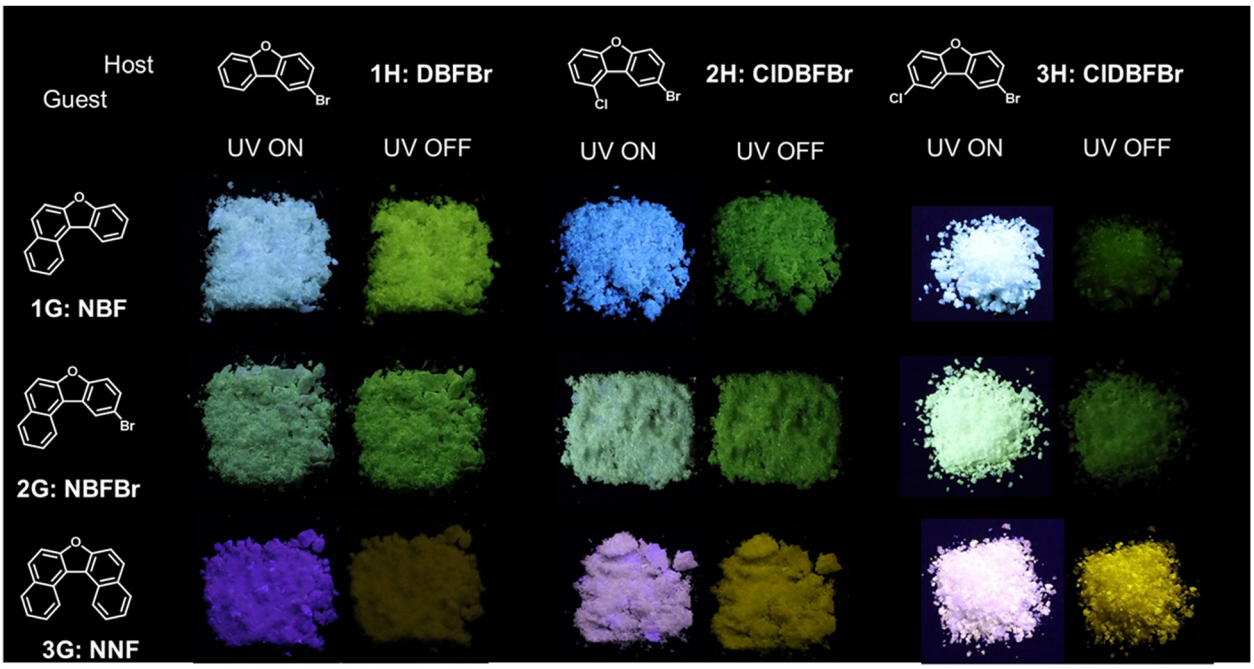


Fig. 1 Luminescent photographs of the host–guest system (guest doping at host with 1% molar ratio) under 254 nm UV light and after removal of the UV irradiation at room temperature. (Inset: Chemical structures of 1H, 2H, 3H, 1G, 2G, and 3G. H represents host and G represents guest).

and (2) how to modulate the dual-mode long-persistence luminescence of the host–guest system.

## Results and discussion

All host and guest molecules utilized in this study are commercially available. Prior to luminescence spectral analysis, rigorous purification methods, including column chromatography and recrystallization, were applied to all samples. High-performance liquid chromatography (HPLC) was also employed to monitor the onset absorption of the aromatic furan derivatives, thereby eliminating the potential for impurity interference with optical properties (Fig. S1–S6, ESI†).[49] For comparative analysis, the absorption and emission spectra of the individual components were examined at room temperature and at 77 K in 2-methyltetrahydrofuran (2-methf) (see Fig. S7 and S8, ESI† and Fig. 2). The UV-visible absorption spectra in solvents of varying polarities (Fig. S7, ESI†) indicate that the longest absorption wavelengths are *circa* 310 nm, 313 nm, and 315 nm for the host molecules (1H, 2H, 3H), and 339 nm, 339 nm, and 354 nm for the guest molecules (1G, 2G, 3G), respectively. These findings correlate with the degree of conjugation. Furthermore, neither the UV absorption (Fig. S7, ESI†) nor the photoluminescence emission (Fig. S8, ESI†) of these host and guest molecules exhibited significant solvatochromic effects, indicating the absence of a charge-transfer state. Subsequently, computational chemistry was employed using TD-DFT at the b3lyp/6-31g(d,p) level in the gas state based on molecular single crystal structures (Fig. 2a, 1G molecule did not obtain a single crystal and its optimized configuration structure was used for calculation), which also primarily displays a π–π* transition mode. The electronic gaps between the highest occupied molecular orbital (HOMO) and the lowest unoccupied molecular orbital (LUMO) of the host [$\Delta E$(H)], and between the HOMO and LUMO of the guest [$\Delta E$(G)], can be approximated as optical gaps of the host and guest molecules, respectively. Our ground-state calculations show that $\Delta E(\mathrm{H}) > \Delta E(\mathrm{G})$ is achieved for high-efficiency host to guest energy transfer.

The steady-state emission spectrum recorded at 298 K (Fig. 2b and c) exhibits maximum emission peaks at wavelengths of 325 nm, 330 nm, 331 nm, 357 nm, 357 nm, and 376 nm, with corresponding lifetimes (Fig. 2d) of 0.23 ns, 0.11 ns, 0.35 ns, 3.44 ns, 0.34 ns, and 2.45 ns, respectively, indicative of typical fluorescence characteristics. The steady-state photoluminescence (PL) and delayed emission (DL) of all host and guest molecules in 2-methf solution at 77 K (Fig. 2b and c) indicate that the energy levels of the lowest excited singlet state ($S_1$) and the lowest excited triplet state ($T_1$) decrease progressively in the following order: 1H $\geq$ 2H > 3H > 1G > 2G > 3G. Which is consistent with the calculated energy levels (Fig. 2g). This ordering suggests that the energy levels of the host and guest molecules are partially aligned, indicating the potential for effective energy transfer. Furthermore, a detailed examination of the UV-visible absorption spectra, steady-state emission at RT and 77 K, and delayed emission spectra of the model compound in the solid state (Fig. S9, ESI†) demonstrated consistency with results obtained from dilutions in 2-methf solution, thereby further substantiating the feasibility of effective energy transfer between the host aggregates and the guest molecules.

Neither the host nor the guest molecules exhibited any significant afterglow in either 2-methf or solid-state powders

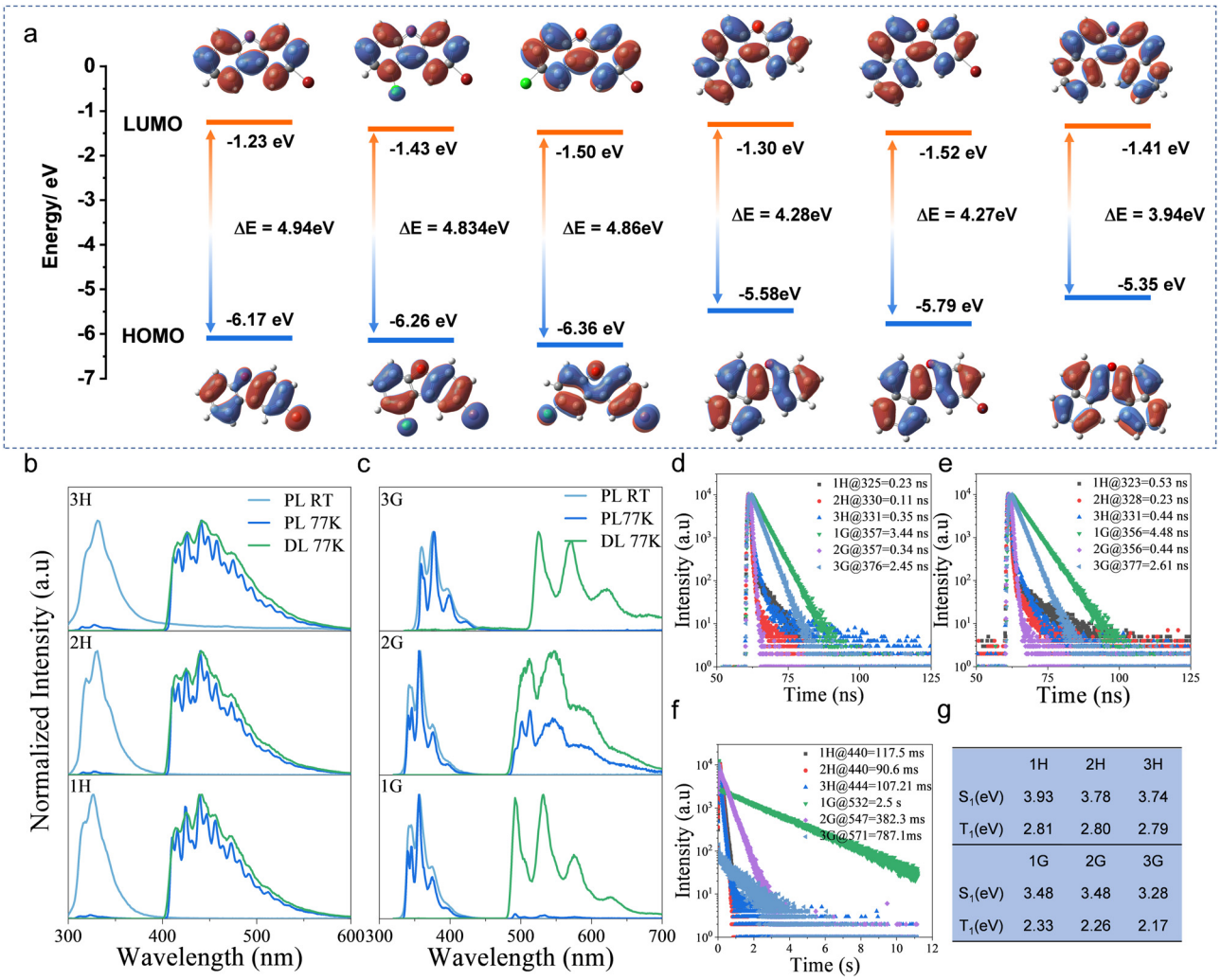


| | 1H | 2H | 3H |
|---|---|---|---|
| $S_1$(eV) | 3.93 | 3.78 | 3.74 |
| $T_1$(eV) | 2.81 | 2.80 | 2.79 |
| | 1G | 2G | 3G |
| $S_1$(eV) | 3.48 | 3.48 | 3.28 |
| $T_1$(eV) | 2.33 | 2.26 | 2.17 |

Fig. 2 (a) Calculations of molecular orbital pairs most significantly involved in an electronic transition from the ground state ($S_0$). Steady-state photoluminescence emission (PL), delayed emission (DL) spectra ((b) and (c), $\lambda_{ex}$ = 285 nm) and emission decay curves (fluorescence lifetime (d) at 298 K; fluorescence lifetime (e) and phosphorescence lifetime (f) at 77 K) of the individual components in dilute 2-methf solutions ($c = 1 \times 10^{-5}$ mol $L^{-1}$) at 298 K and 77 K. (g) Calculated energy levels of the lowest excited single state ($S_1$) and the lowest excited triplet state ($T_1$) for monomer.

at room temperature, phosphorescence only occurs at 77 K (Fig. 2f), suggesting an extremely low intrinsic RTP yield among all single component samples. However, after doping trace amounts of guest molecules into the host, upon removal of 254 nm UV irradiation, a pronounced afterglow (Fig. 1) was observed in the host–guest samples prepared through evaporative drying from solutions in $CH_2Cl_2$ or $CHCl_3$, demonstrating the presence of room-temperature phosphorescence (RTP) properties, and the RTP likely originates from host–guest energy transfer. The concentration of guest molecules is crucial to the RTP performance. Accordingly, a series of host–guest materials with molar ratios ranging from 1000 : 1 to 20 : 1 were prepared and studied (Fig. S10–S12, ESI†). As the concentration of guest molecules increased, all host–guest samples exhibited noticeable visible afterglow; the sample with the intensest room-temperature phosphorescence generally appears at a doping concentration of 1%, The optimal doping concentration was determined to be 1%, which balances efficient energy transfer and minimizes concentration quenching. At this concentration, guest molecules are sufficiently dispersed within the host matrix, facilitating effective host-to-guest energy transfer while preventing aggregation-induced quenching that occurs at higher concentrations, while the phosphorescence emission wavelengths and vibrational structures remained largely unchanged. The lifespan in the 480–750 nm region ranges from 50 ms to 229 ms, indicating long-persistence property (Fig. 1 and Fig. S13–S15, ESI†). We also noticed that the existence of delayed luminescence in the 320–480 nm region, and the intensities and lifetimes of the delayed emission vary significantly among different doped samples (Fig. S13–S15, ESI†), which will be the focus of the following discussion. Given the exceptional phosphorescence performance of samples with 1% guest molecules dispersed in the host matrix, these samples were selected for further photophysical investigation. Notably, the powder X-ray diffraction patterns (Fig. S17 and S18, ESI†) of the host–guest doping samples reveal sharp peaks indicative of

 

good crystallinity. The diffraction patterns closely resemble the superposition of pure host and guest, with no additional peaks or shifts in diffraction angles, suggesting that a small amount of guest molecules is embedded in the host crystal lattice.

Fig. 1 presents the fluorescence and phosphorescence images of 1% doped samples under UV illumination and subsequent cessation of UV irradiation. All the doped samples exhibit long-persistence afterlow with varying intensities. In the first row of Fig. 1, three host–guest powders incorporating the 1G molecule (entitled "1G-based system/sample") exhibit a distinct green afterglow lasting several seconds following the removal of the UV source. Notably, although the 2H/1G and 3H/1G system contain a more abundant heavy atom (2H and 3H have an additional Cl atom) environment compared to 1H/1G, its afterglow intensity is slightly diminished, likely due to dominated non-radiative decay processes from double C-halogen bonds.[6] Moreover, 2H and 3H are isomers, but the steady-state emission color in the 2H/1G differs from 3H/1G, which is white-light emission that could be useful in purely organic LED applications,[50] suggestting the impact of heavy atom substitution sites on the conjugation degree of the host molecules. Additionally, in the second row of Fig. 1, three host–guest samples based on the 2G molecule also demonstrate a pronounced green delayed emission. Although the 2G molecule contains an additional heavy bromine atom compared to the 1G molecules, the delayed emission brightness of the host/2G material is again slightly lower than that of the host/1G material. Furthermore, in the third row, the red-shifted yellow afterglow of the host/3G materials is clearly observed, attributed to the maximum conjugation degree of the 3G molecule.

Fig. 3a–i illustrates the prompt (steady-state photoluminescence emission, PL) and delayed emission (DL) spectra of all nine 1% doped host–guest samples. For the 1G-(3a–c) and 2G-based (3d–f) systems, the PL emission spectra are similar, spanning approximately 320–480 nm and 480–750 nm, which is rational for prompt emission spectra to come from both individual host and guest components and the host–guest complex components. Notably, the 1G-based samples exhibit stronger emissions in the 320–480 nm region compared to the 2G samples. However, the delayed emission spectrum (DL) of host/1G differs significantly from that of host/2G, with host/1G demonstrating a much more pronounced emission signal in the shorter wavelength band of 340–470 nm, although the

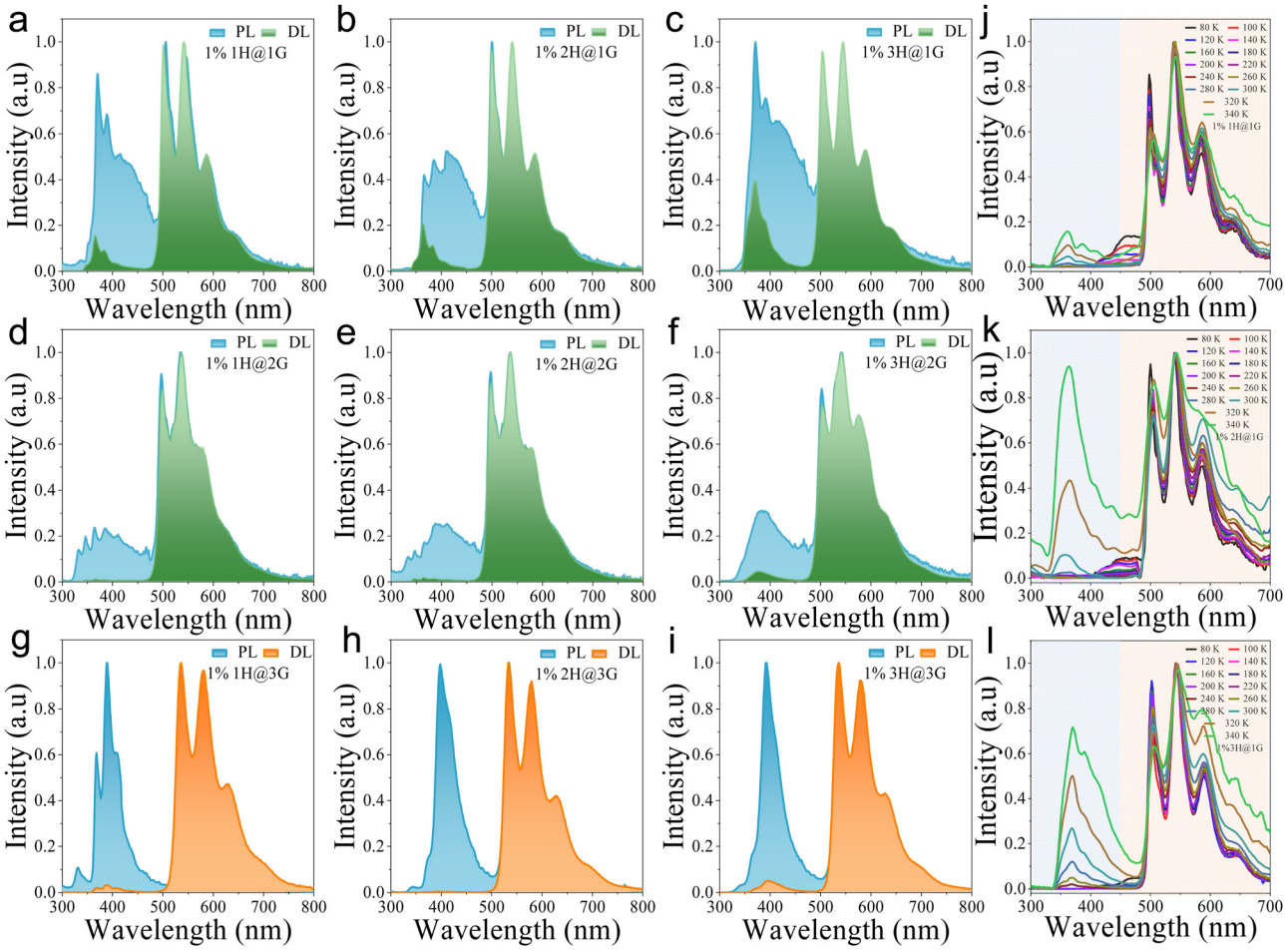


Fig. 3 Steady-state photoluminescence emission (PL) and delayed luminescence emission (DL) spectra ($\lambda_{ex}$ = 285 nm) of host–guest systems in solid-states at 298 K (1G-based samples: (a)–(c); 2G-based samples: (d)–(f); 3G-based samples: (g)–(i)). Temperature-dependent delayed emission (TDDE) spectra of the host–guest samples ((j)–(l) 1G-based samples) for dual-mode long-persistence afterglow, from 80 K to 340 K with 20 K interval.

longer wavelength emission band at 480–750 nm is similar. What is the shorter wavelength delayed luminescence and why do 1G- and 2G-based samples perform differently? Fig. S13–S15 (ESI†) presents the delayed lifetime decay profiles of all host–guest samples. The shorter wavelength lifetimes for host/1G and host/2G are also slightly shorter (Table S1, ESI,† 49.00 ms, 49.29 ms, 8.26 ms, 21.38 ms, 18.92 ms, and 6.14 ms), while the lifetimes for the longer wavelength delayed emissions of host/1G and host/2G are significantly extended (Table S5, ESI,† 208.51 ms, 206.08 ms, 83.01 ms, 90.65 ms, 88.69 ms, and 62.12 ms). This indicates that the two emission bands result from distinct excitation decay mechanisms. After comparing DL with the spectra of the model compounds both in the solid state and in the solution mentioned above, We speculate the shorter wavelength emissions to TADF, which most likely arises from reverse intersystem crossing from the excited triplet state of the guest molecules to the excited singlet state of the host–guest complex. While triplet–triplet annihilation (TTA) could also contribute to delayed emission, several factors in our system suggest that TADF is the predominant mechanism, (1) emission characteristics: the spectral shape and temperature dependence of the delayed emission are consistent with typical TADF behavior observed in similar host–guest systems. (2) lifetime data: the lifetimes of the delayed emissions do not exhibit the strong concentration dependence typically associated with TTA. (3) Energy gap considerations: the energy gap between the triplet and singlet states is optimized to facilitate RISC, which is a hallmark of TADF mechanisms. These observations collectively support the assignment of the delayed emission to TADF rather than TTA. To confirm our conjecture, a temperature-dependent delayed emission (TDDE) spectra test was conducted. As depicted in Fig. 3j–l for the 1G-based sample, the proportion of delayed components significantly increases with rising temperature, indicating the uphill nature of reverse intersystem crossing in TADF.[20] 2G- and 3G-based samples also possess certain TADF of varying degrees (Fig. S19 and S20, ESI†). Moreover, the shorter wavelength delayed emission is not observed in the individual components, suggesting that the TADF emission is indeed a product of the host–guest complex components. Additionally, the longer wavelength delayed emission bands of the host/guest materials can be attributed to RTP from the excited triplet state of the guest molecules. Accordingly, dual-mode (both RTP and TADF) long-persistence afterglow has been achieved in this aromatic furan organic host–guest system, with TADF of approximately 50 ms.

A schematic illustration is provided to elucidate the mechanism underlying this dual-mode long-persistence afterglow (Fig. 4b). Specifically, the photon energy is first converted to triplet excitons of the hosts from the intersystem crossing process (ISC, which could be accelerated by the heavy-atom effect); then the guest molecules capture triplet excitons from the excited triplet state of the host through energy transfer, resulting in phosphorescence emission; subsequently, the triplet excitons of the guest can transition to the excited singlet state of the host–guest complex *via* reverse intersystem crossing (RISC), thereby emitting TADF.

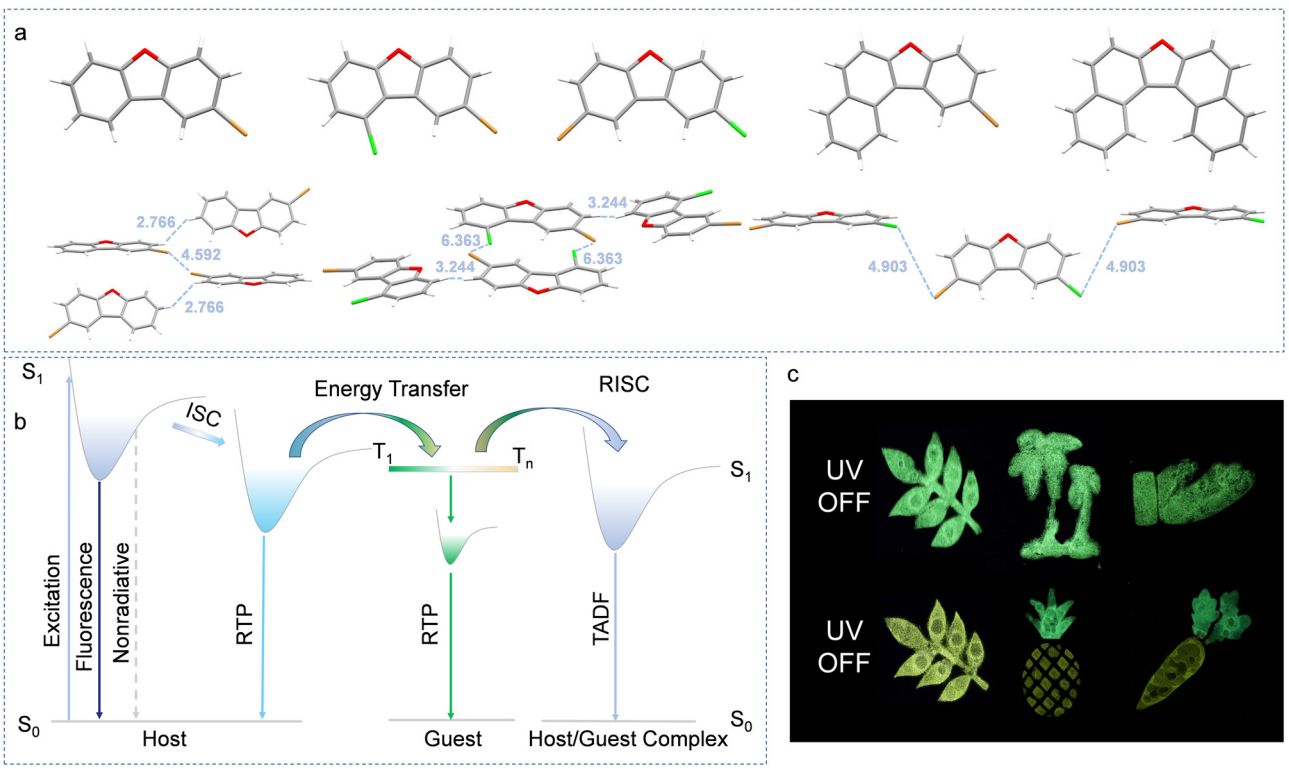


Fig. 4 (a) Single-crystal X-ray diffraction data of the single host and guest molecules. (b) Proposed mechanism of the dual-mode long-persistence afterglow. (c) Encryption illustration of the host–guest samples as a ink material. The figure shows the image after the ultraviolet light was turned off.

 

We also observed that the heavy-atom effect of the host and guest molecules plays distinct roles in facilitating TADF. For instance, the proportion of TADF increases from 1H to 3H in 1G-based samples (Fig. 3a–c), as the additional heavy atom in 2H and 3H significantly enhances the intersystem crossing (ISC) process. This leads to a higher population of triplet excitons in the host, which then transfer to the guest molecule, resulting in TADF. In contrast, when a heavy atom is attached to the guest molecule, as is the case for 2G-based samples (Fig. 3d–f), the TADFs are less than 1G-based samples because the heavy atoms in the 2G molecule notably expedite both the radiative process ($k_r$) and non-radiative decay process ($k_{nr}$) for guests, which is supported by the shorter RTP lifetimes observed for 2G-based samples (Table S5–S8, ESI†). As a result, the reverse intersystem crossing (RISC) process becomes less competitive, leading to reduced TADF generation. Additionally, 3H/1G has more TADF than 2H/1G, although 2H and 3H are isomers, which could be explained by 3H having a more tight packing mode and facilitating the energy transfer and all radiative and non-radiative processes. As indicated by the single crystal X-ray diffraction data (Fig. 4a and Tables S9, S10, ESI†), the distances between heavy atoms in the 1H, 2H, and 3H molecules are measured at 4.5 Å, 6.3 Å, and 4.9 Å, respectively. The tighter arranged molecular crystals of 3H contribute to a redshift (approximately 6 nm) in the solid-state delayed emission spectra, also producing more TADF but with shorter lifetimes (Fig. 3a–c and Table S1, ESI†).

In the 3G-based system (Fig. 3g–i), persistent yellow room-temperature phosphorescence (RTP) is observed. Despite the absence of a heavy atom in the 3G guest (similar to the 1G), the delayed emission spectra of the host/3G exhibit a much weaker TADF signal in the shorter wavelength range of 340–470 nm. This is attributed to larger energy gaps between the excited triplet state of the guest (3G) and the host molecules, as well as between the excited singlet state of the host–guest complex. As a result, triplet energy transfer is less efficient, and also the majority of the triplet excitons in the guest contribute to the yellow phosphorescence, while only a limited number of excitons undergo reverse intersystem crossing to transition to the excited singlet state of the host–guest complex and emit TADF. This explanation is supported by the data that the TADF lifetimes of the host/3G samples are significantly shorter (Table S1, 71.95 μs, 83.26 μs, and 4.07 ms, ESI†) compared to the host/1G and host/2G systems, particularly in the case of the 1H and 2H samples, where the lifetimes are at least two orders of magnitude shorter. In contrast, the RTP is less affected, and the RTP lifetimes of the host/3G system (Table S5, 155.92 ms, 117.98 ms, and 138.75 ms, ESI†) are comparable to those of the host/1G and host/2G systems. Thus, the dual-mode long-persistence luminescence of the host–guest system can be effectively modulated by adjusting the energy gaps between the host and guest molecules. This study suggests that to enhance TADF efficiency in a host–guest system, the energy level difference between the host and guest should not be too large, and the incorporation of a heavy atom into the host molecule is beneficial.

The aromatic furan organic host–guest system also displays a color-tunable character, as shown in 2D steady-state PL spectra (Fig. S21–S29, ESI†). When exciting the doped samples with different excitation wavelengths from 240 nm to 360 nm, the sample could display fluorescence, TADF, and RTP with different intensities and ratios, especially in 1H/1G, 1H/3G, 2H/1G, and 3H/3G samples, which have the potential for excitation-dependent display applications.[51–56] Furthermore, we demonstrated an application utilizing inkjet printing based on two host–guest combinations, 1H/1G (1% doped) and 2H/3G (1%). These combinations yield bright green and yellow afterglows (Fig. 4c), respectively, upon cessation of excitation. The color display application leverages the excellent RTP properties of the host guest samples have been successfully realized through inkjet printing, potentially facilitating the commercialization of RTP materials.

## Conclusions

In summary, we have developed a host–guest doping system exhibiting dual-mode long-persistence afterglow, characterized by highly efficient RTP with lifetimes exceeding 200 ms and TADF with a lifetime of approximately 50 ms. This phenomenon can be attributed to the modulation of the competition rates between intersystem crossing (ISC) and reverse intersystem crossing (RISC) processes within the host–guest system, with these rates being influenced by the heavy-atom effects in both the host and guest molecules. The findings presented herein offer valuable insights for the design of high-efficiency dual-mode long-persistence afterglow materials and may serve as a useful reference for achieving efficient room-temperature phosphorescence in organic host–guest systems.

## Data availability

The data supporting this article have been included as part of the ESI.†

## Conflicts of interest

There are no conflicts to declare.

## Acknowledgements

This work was financially supported by the National Natural Science Foundation of China (grant no. 21975238, 22103077, 22273097 and 22003063) and University of Science and Technology of China (2021ZD0303301, KY9990000139 and YD9990002010).

## References

1 A. Jain, A. Kumar, S. J. Dhoble and D. R. Peshwe, Persistent luminescence: an insight, *Renewable Sustainable Energy Rev.*, 2016, **65**, 135–153.
2 X. Chen, W. Dai, X. Wu, H. Su, C. Chao, Y. Lei, J. Shi, B. Tong, Z. Cai and Y. Dong, Fluorene-based host-guest phosphorescence materials for information encryption, *Chem. Eng. J.*, 2021, **426**, 131607.

3 Y. Yang, Y. Liang, Y. Zheng, J. Li, S. Wu, H. Zhang, T. Huang, S. Luo, C. Liu, G. Shi, F. Sun, Z. Chi and B. Xu, Efficient and color-tunable dual-mode afterglow from large-area and flexible polymer-based transparent films for anti-counterfeiting and information encryption, *Angew. Chem., Int. Ed.*, 2022, **61**, e202201820.
4 Q. Dang, Y. Jiang, J. Wang, Q. Zhang, M. Zhang, S. Luo, Y. Xie, K. Pu, Q. Li and Z. Li, Room-temperature phosphorescence resonance energy transfer for construction of near-infrared afterglow imaging agents, *Adv. Mater.*, 2020, **32**, 2006752.
5 Y. Wang, H. Gao, J. Yang, M. Fang, D. Ding, B. Tang and Z. Li, High performance of simple organic phosphorescence host-guest materials and their application in time-resolved bioimaging, *Adv. Mater.*, 2021, **33**, 2007811.
6 R. Kabe and C. Adachi, Organic long persistent luminescence, *Nature*, 2017, **550**, 384–387.
7 X. Ma, J. Wang and H. Tian, Assembling-induced emission: an efficient approach for amorphous metal-free organic emitting materials with room-temperature phosphorescence, *Acc. Chem. Res.*, 2019, **52**, 738–748.
8 C. Chiatti, C. Fabiani and A. Pisello, Long persistent luminescence: A road map toward promising future developments in energy and environmental science, *Annu. Rev. Mater. Res.*, 2021, **51**, 409–433.
9 H. Gao and X. Ma, Recent progress on pure organic room temperature phosphorescent polymers, *Aggregate*, 2021, **2**, e38.
10 J. Guo, C. Yang and Y. Zhao, Long-lived organic room-temperature phosphorescence from amorphous polymer systems, *Acc. Chem. Res.*, 2022, **55**, 1160–1170.
11 L. Liang, J. Chen, K. Shao, X. Qin, Z. Pan and X. Liu, Controlling persistent luminescence in nanocrystalline phosphors, *Nat. Mater.*, 2023, **22**, 289–304.
12 L. Wang, J. Miao, Y. Zhang, C. Wu, H. Huang, X. Wang and C. Yang, Discrete Mononuclear Platinum (II) Complexes Realize High-Performance Red Phosphorescent OLEDs with EQEs of up to 31.8% and Superb Device Stability, *Adv. Mater.*, 2023, **35**, 2303066.
13 J. Yang, M. Fang and Z. Li, Stimulus-responsive room temperature phosphorescence in purely organic luminogens, *InfoMat*, 2020, **2**, 791–806.
14 X. Wang, H. Shi, H. Ma, W. Ye, L. Song, J. Zan, X. Yao, X. Ou, G. Yang, Z. Zhao, M. Singh, C. Lin, G. Zhang, Z. An, X. Liu and W. Huang, Organic Phosphors with Bright Triplet Excitons for Efficient X-Ray-Excited Luminescence, *Nat. Photonics*, 2021, **15**, 187–192.
15 R. Gao, M. S. Kodaimati and D. Yan, Recent advances in persistent luminescence based on molecular hybrid materials, *Chem. Soc. Rev.*, 2021, **50**, 5564–5589.
16 Q. Zhou, C. Yang and Y. Zhao, Dynamic organic room-temperature phosphorescent systems, *Chem*, 2023, **9**, 2446–2480.
17 G. Zhang, G. M. Palmer, M. W. Dewhirst and C. L. Fraser, A dual-emissive-materials design concept enables tumour hypoxia imaging, *Nat. Mater.*, 2009, **8**, 747–751.
18 X. Wang and K. Pu, Molecular substrates for the construction of afterglow imaging probes in disease diagnosis and treatment, *Chem. Soc. Rev.*, 2023, **52**, 4549–4566.
19 O. Bolton, K. Lee, H. J. Kim, K. Y. Lin and J. Kim, Activating Efficient Phosphorescence from Purely Organic Materials by Crystal Design, *Nat. Chem.*, 2011, **3**, 205–210.
20 H. Uoyama, K. Goushi, K. Shizu, H. Nomura and C. Adachi, Highly Efficient Organic Light-Emitting Diodes from Delayed Fluorescence, *Nature*, 2012, **492**, 234–238.
21 X. Ai, E. W. Evans, S. Dong, A. J. Gillett, H. Guo, Y. Chen, T. J. H. Hele, R. H. Friend and F. Li, Efficient Radical-Based Light-Emitting Diodes with Doublet Emission, *Nature*, 2018, **563**, 536–540.
22 X. Wang, Y. Sun, G. Wang, J. Li, X. Li and K. Zhang, TADF-Type Organic Afterglow, *Angew. Chem., Int. Ed.*, 2021, **60**, 17138–17147.
23 H. Zhang, M. Zhang and C. Zheng, An organic dimer with TADF-type electroexcitation afterglow, *Matter*, 2023, **6**, 1055–1057.
24 K. Wan, B. Tian, Y. Zhai, Y. Liu, H. Wang, S. Liu, S. Li, W. Ye, Z. An, C. Li, J. Li, T. D. James and Z. Chen, Structural materials with afterglow room temperature phosphorescence activated by lignin oxidation, *Nat. Commun.*, 2022, **13**, 5508.
25 Y. Fan, S. Liu, M. Wu, L. Xiao, Y. Fan, M. Han, K. Chang, Y. Zhang, X. Zhen and Z. Li, Mobile Phone Flashlight-Excited Red Afterglow Bioimaging, *Adv. Mater.*, 2022, **34**, 2201280.
26 Z. Wang, A. Li, Z. Zhao, T. Zhu, Q. Zhang, Y. Zhang, Y. Tan and W. Z. Yuan, Accessing Excitation-and Time-Responsive Afterglows from Aqueous Processable Amorphous Polymer Films through Doping and Energy Transfer, *Adv. Mater.*, 2022, **34**, 2202182.
27 W. Dai, X. Niu, X. Wu, Y. Ren, Y. Zhang, G. Li, H. Su, Y. Lei, J. Xiao, J. Shi, B. Tong, Z. Cai and Y. Dong, Halogen bonding: a new platform for achieving multi-stimuli-responsive persistent phosphorescence, *Angew. Chem., Int. Ed.*, 2022, **61**, e202200236.
28 X. Yang, G. Waterhouse, S. Lu and J. Yu, Recent advances in the design of afterglow materials: mechanisms, structural regulation strategies and applications, *Chem. Soc. Rev.*, 2023, **52**, 8005–8058.
29 B. Chen, W. Huang, X. Nie, F. Liao, H. Miao, X. Zhang and G. Zhang, An organic host-guest system producing room-temperature phosphorescence at the parts-per-billion level, *Angew. Chem., Int. Ed.*, 2021, **60**, 16970–16973.
30 J. Yang, X. Zhen, B. Wang, X. Gao, Z. Ren, J. Wang, Y. Xie, J. Li, Q. Peng, K. Pu and Z. Li, The influence of the molecular packing on the room temperature phosphorescence of purely organic luminogens, *Nat. Commun.*, 2018, **9**, 840.
31 W. Yuan, X. Shen, H. Zhao, J. W. Y. Lam, L. Tang, P. Lu, C. Wang, Y. Liu, Z. Wang, Q. Zheng, J. Sun, Y. Ma and B. Z. Tang, Crystallization-induced phosphorescence of pure organic luminogens at room temperature, *J. Phys. Chem. C*, 2010, **114**, 6090–6099.
32 Z. Lin, R. Kabe, K. Wang and C. Adachi, Influence of energy gap between charge-transfer and locally excited states on organic long persistence luminescence, *Nat. Commun.*, 2020, **11**, 191.
33 X. Zhang, L. Du, W. Zhao, Z. Zhao, Y. Xiong, X. He, P. Gao, P. Alam, C. Wang, Z. Li, J. Leng, J. Liu, C. Zhou, J. Lam,

 

D. Phillips, G. Zhang and B. Tang, Ultralong UV/mechano-excited room temperature phosphorescence from purely organic cluster excitons, *Nat. Commun.*, 2019, **10**, 5161.

34 W. Wang, Y. Zhang and W. J. Jin, Halogen bonding in room-temperature phosphorescent materials, *Coord. Chem. Rev.*, 2020, **404**, 213107.

35 W. Ye, H. Ma, H. Shi, H. Wang, A. Lv, L. Bian, M. Zhang, C. Ma, K. Ling, M. Gu, Y. Mao, X. Yao, Z. An, X. Liu and W. Huang, Confining isolated chromophores for highly efficient blue phosphorescence, *Nat. Mater.*, 2021, **20**, 1539–1544.

36 H. Suo, X. Zhang and F. Wang, Controlling X-ray-activated persistent luminescence for emerging applications, *Trends Chem.*, 2022, **4**, 726–738.

37 W. Zhao, Z. He and B. Z. Tang, Room-temperature Phosphorescence from Organic Aggregates, *Nat. Rev. Mater.*, 2021, **5**, 869–885.

38 Z. Man, Z. Lv, Z. Xu, J. He, Q. Liao, Y. Yang, J. Yao and H. Fu, Host Surface-Induced Excitation Wavelength-Dependent Organic Afterglow, *J. Am. Chem. Soc.*, 2023, **145**, 13392–13399.

39 J. You, X. Zhang, Q. Nan, K. Jin, J. Zhang, Y. Wang, C. Yin, Z. Yang and J. Zhang, Aggregation-regulated room-temperature phosphorescence materials with multi-mode emission, adjustable excitation-dependence and visible-light excitation, *Nat. Commun.*, 2023, **14**, 4163.

40 X. Yang, S. Wang, K. Sun, H. Liu, M. Ma, S. T. Zhang and B. Yang, A Heavy-atom-free Molecular Motif Based on Centrosymmetric Bird-like Structured Tetraphenylenes with Room-Temperature Phosphorescence (RTP) Afterglow over 8 s, *Angew. Chem., Int. Ed.*, 2023, **62**, e2023064.

41 K. Chang, L. Xiao, Y. Fan, J. Gu, Y. Wang, J. Yang, M. Chen, Y. Zhang, Q. Li and Z. Li, Lighting up metastasis process before formation of secondary tumor by phosphorescence imaging, *Sci. Adv.*, 2023, **9**, eadf6757.

42 X. Sun, B. Zhang, X. Li, C. O. Trindle and G. Zhang, External heavy-atom effect via orbital interactions revealed by single-crystal X-ray diffraction, *J. Phys. Chem. A*, 2016, **120**, 5791–5797.

43 J. Xu, X. Wu, J. Li, Z. Zhao and B. Z. Tang, Regulating Photophysical Property of Aggregation-Induced Delayed Fluorescence Luminogens via Heavy Atom Effect to Achieve Efficient Organic Light-Emitting Diodes, *Adv. Opt. Mater.*, 2022, **10**, 2102568.

44 G. Pan, Z. Yang, H. Liu, Y. Wen, X. Zhang, Y. Shen, C. Zhou, S. T. Zhang and B. Yang, Folding-Induced Spin-Orbit Coupling Enhancement for Efficient Pure Organic Room-Temperature Phosphorescence, *J. Phys. Chem. Lett.*, 2022, **13**, 1563–1570.

45 Z. Xiong, W. Gong, P. Xu, M. Jiang, X. Cai, Y. Zhu, X. Ping, H. Feng, H. Ma and Z. Qian, Reexamining the heavy-atom-effect: the universal heavy-atom induced fluorescence enhancement principle for through-space conjugated AIE-gens, *Chem. Eng. J.*, 2023, **451**, 139030.

46 B. Chen, W. Huang and G. Zhang, Observation of chiral-selective room-temperature phosphorescence enhancement via chirality-dependent energy transfer, *Nat. Commun.*, 2023, **14**, 1514.

47 S. Li, L. Fu, X. Xiao, H. Geng, Q. Liao, Y. Liao and H. Fu, Regulation of Thermally Activated Delayed Fluorescence to Room-Temperature Phosphorescent Emission Channels by Controlling the Excited-States Dynamics via J- and H-Aggregation, *Angew. Chem., Int. Ed.*, 2021, **60**, 18059–18064.

48 Y. Wang, M. Gao, J. Ren, J. Liang, Y. Zhao, M. Fang, J. Yang and Z. Li, Exciplex-induced TADF, persistent RTP and ML in a host-guest doping system, *Mater. Chem. Front.*, 2023, **7**, 1093–1099.

49 C. Chen, Z. Chi, K. C. Chong, A. S. Batsanov, Z. Yang, Z. Mao, Z. Yang and B. Liu, Carbazole Isomers Induce Ultralong Organic Phosphorescence, *Nat. Mater.*, 2021, **20**, 175–180.

50 Z. Chen, C. L. Ho, L. Wang and W. Y. Wong, Single-Molecular White-Light Emitters and Their Potential WOLED Applications, *Adv. Mater.*, 2020, **32**, 1903269.

51 S. Reineke, N. Seidler, S. R. Yost, F. Prins, W. A. Tisdale and M. A. Baldo, Highly efficient, dual state emission from an organic semiconductor, *Appl. Phys. Lett.*, 2013, **103**(9), 093302.

52 Y. Gong, L. Zhao, Q. Peng, D. Fan, W. Yuan, Y. Zhang and B. Tang, Crystallization-induced dual emission from metal- and heavy atom-free aromatic acids and esters, *Chem. Sci.*, 2015, **6**, 4438–4444.

53 L. Wei, S. Guo, B. Zhang, B. Jiang, Y. Wang, Z. Liu, Y. Xu, Y. Gong, Y. Liu and W. Z. Yuan, Tuning Circularly Polarized Afterglow Color via Modulation of Energy and Chirality Transfer in Co-Doped Films, *Adv. Funct. Mater.*, 2024, **34**, 2409681.

54 M. Gao, J. Ren, Y. Gong, M. Fang, J. Yang and Z. Li, A new insight into aggregation structure of organic solids and its relationship to room-temperature phosphorescence effect, *Aggregate*, 2024, **5**, e462.

55 Q.-Q. Xia, X.-H. Wang, J.-L. Yu, Z.-Y. Chen, X.-Y. Lou, X. Liu, M.-X. Wu and Y.-W. Yang, Smart phosphorescence from solid to water through progressive assembly strategy based on dual phosphorescent sources, *Aggregate*, 2023, **4**, e370.

56 S. Cai, X. Yao, H. Ma, H. Shi and Z. An, Manipulating intermolecular interactions for ultralong organic phosphorescence, *Aggregate*, 2023, **4**, e320.